Available online at www.sciencedirect.com
SCIENCE DIRECT®
Journal of Solid State Chemistry 177 (2004) 3099–3104
JOURNAL OF SOLID STATE CHEMISTRY
http://elsevier.com/locate/jssc

Neutron diffraction study, magnetism and magnetotransport of stoichiometric $CaVO_3$ perovskite with positive magnetoresistance

H. Falcón, J.A. Alonso,* M.T. Casais, M.J. Martínez-Lope, and J. Sánchez-Benítez

Instituto de Ciencia de Materiales de Madrid, CSIC, Cantoblanco, 28049 Madrid, Spain

Received 9 February 2004; received in revised form 27 April 2004; accepted 7 May 2004

Available online 8 July 2004

Abstract

A stoichiometric calcium vanadium (IV) oxide with formula $CaVO_3$ has been prepared by soft-chemistry procedures, followed by annealing under reducing conditions (H_2/N_2 flow). This material has been studied by X-ray and neutron powder diffraction (NPD), thermal analysis, magnetic and magnetotransport measurements. $CaVO_{3.0}$ perovskite crystallizes in the orthorhombic *Pbnm* (No. 57) space group, with the $GdFeO_3$-type structure. The unit-cell parameters are $a = 5.3219(1)$ Å, $b = 5.3427(1)$ Å and $c = 7.5472(1)$ Å. In this distorted perovskite the VO_6 octahedra are tilted by 10.1° in order to optimize the Ca–O bond-lengths. A bond valence study from NPD data confirms the tetravalent oxidation state for V cations. The perovskite is fully oxygen stoichiometric, as demonstrated from thermal analysis and the refinement of the oxygen occupancy factors. The magnetic susceptibility is predominantly Pauli paramagnetic-like, although a non-negligible temperature-dependent component due to isolated V^{4+} spins is patent at low temperatures. The transport measurements show a metallic behavior between 2 and 300 K; at low temperatures a positive magnetoresistance as large as 14% for $H = 9$ T is interpreted as the result of quantum interference effects.

Keywords: Calcium vanadium oxide; Neutron powder diffraction; Perovskite structure; Pauli paramagnetism; Positive magnetoresistance

1. Introduction

Perovskite-type transition metal oxides with $3d^1$ and related configurations, containing narrow bands of $3d$ parentage, are particularly susceptible to correlation effects, leading to exciting phenomena such as high-temperature superconductivity [1], in $3d^9$ cuprates (hole-symmetric to a $3d^1$ system) or colossal magnetoresistance [2] in $LaMnO_3$-related perovskites (Jahn–Teller distorted $t_{2g}^3 eg^1$ system). Some of these $3d^1$ systems are close to a Mott transition [3] (a metal–insulator transition driven by electron–electron interactions) such as $LaTiO_3$, which can be either a Mott–Hubbard-type insulator or a metal depending on subtle changes in the oxygen stoichiometry and, thus, on the oxidation state of Ti cations.

Another paradigmatic example is $CaVO_3$, which lies just on the metallic side of the Mott transition. Also depending on the preparation procedure, crystalline conformation and oxygen stoichiometry, this interesting material has been described as a metal, with a resistivity as low as $10^{-4}\,\Omega$ cm [4] or an insulator, in oxygen understoichiometric and even over-stoichiometric compositions [5]. In fact, the described physical properties and crystal structures of $CaVO_3$ have been controversial during the last 30 years.

$CaVO_3$ was first described by Chamberland et al. in 1971 [6], as a metallic conductor exhibiting Pauli paramagnetism. These authors prepared a polycrystalline phase by solid-state reaction from VO_2 and CaO under high-pressure conditions (60–65 kbar). It was described as an orthorhombically distorted perovskite, with $a = 5.4215(8)$ Å, $b = 5.3353(9)$ Å, $c = 7.5406(8)$ Å; the metallic and Pauli paramagnetic behavior being consistent with a delocalized d^1 electron system, as proposed by Goodenough [7] for perovskite-type compounds having one electron system such as Ti^{3+} or Re^{6+}. The oxygen non-stoichiometric compound $CaVO_{3-\delta}$ was subsequently reported by Iga et al. [4] on

*Corresponding author. Fax: +34-913720623.
E-mail address: ja.alonso@icmm.csic.es (J.A. Alonso).

0022-4596/$ - see front matter © 2004 Elsevier Inc. All rights reserved.
doi:10.1016/j.jssc.2004.05.010

single crystal materials annealed under different atmospheres. They reported a metallic behavior in reduced samples ($CaVO_{2.7}$), with a transition to an insulating character when annealing in O_2 to give the stoichiometric $CaVO_3$ compound. Thereafter, Inoue et al. [8] of the same group reported that $CaVO_3$ is metallic and that slightly oxidized it is an insulator ($CaVO_{3.05}$). Subsequently, Fukushima et al. [9] described, also for single crystals, that the slightly deficient $CaVO_{2.98}$ is cubic, with a lattice parameter of 3.79 Å, whereas the off-stoichiometric $CaVO_{3-\delta}$ with superior δ values is orthorhombic. Recently, three new $CaVO_{3-\delta}$ phases with a vacancy ordered structure and a much larger unit-cell than the primitive one have been reported [10]; these oxygen-deficient phases are unstable in air and easily oxidized to $CaVO_{3.00}$. The oxygen-defective phases present a Curie–Weiss behavior, while $CaVO_{3.00}$ is a Pauli paramagnet [10].

As shown, the data reported on $CaVO_{3-\delta}$ are complicated and scattered over various oxygen non-stoichiometries and structures. One reason for this is the difficulty of systematically controlling the oxygen content during synthesis. Also, the rough estimation of oxygen stoichiometry and insufficient identification of the crystal structures contribute to scatter the reported data.

Aiming to contribute to clarify the oxygen stoichiometry to crystal-structure relationship, in this paper we describe the characterization from neutron powder diffraction (NPD) data of a stoichiometric $CaVO_{3.00}$ material, prepared by soft-chemistry procedures. We also report on the magnetic and electrical properties for this stoichiometric perovskite, for which we describe positive magnetoresistance at low temperatures.

2. Experimental

$CaVO_3$ material was obtained in powder form by a citrate technique. Stoichiometric amounts of analytical grade $CaCO_3$ and VO_3NH_4 were dissolved in citric acid. The solution was slowly evaporated, leading to an organic resin which was dried at 120°C and slowly decomposed at temperatures up to 600°C. The sample was then heated at 800°C for 2 h in order to eliminate all the organic materials and nitrates. The black precursor powders, very reactive, were then reduced at 900°C, H_2/N_2 (5%/95%) flow for 12 h.

The reaction products were characterized by X-ray diffraction (XRD) for phase identification and to assess phase purity. XRD analysis was performed using a Siemens D501 diffractometer controlled by a DACO-MP computer using Ni filtered Cu$K\alpha$ radiation ($\lambda = 1.5406$ Å). The diffraction patterns were recorded in the 2Θ range 10–100 in steps of 0.05°. A room-temperature NPD pattern was collected in the high-resolution D2B diffractometer at the ILL-Grenoble with a wavelength of 1.594 Å, selected from a Ge monochromator. The high-flux mode was used. About 4 g of sample was contained in a vanadium can; a collecting time of 3 h was required to collect a full diffraction pattern.

The NPD data were analyzed by the Rietveld method, using the FULLPROF program [11]. The line shape of the diffraction peaks was generated by a pseudo-Voigt function, and the background refined to a fifth-degree polynomial. The coherent scattering lengths for Ca, V and O were, respectively, 4.70, −0.382 and 5.803 fm. In the final run the following parameters were refined: background coefficients, zero-point, half-width, pseudo-Voigt and asymmetry parameters for the peak shape; scale factor, positional, occupancy factors for oxygen atoms, and unit-cell parameters. The thermal factor for V was fixed to 0.3 $Å^2$ and was not refined given the small scattering power of this element; the remaining isotropic thermal factors were refined.

Thermal analysis was carried out in a Mettler TA3000 system equipped with a TC10 processor unit. Thermogravimetric profiles were obtained in a TG50 microbalance operating at 1 μg accuracy. About 40 mg of the sample was heated in air flow at 5 K/min up to 1173 K.

The magnetic susceptibility was measured with a commercial SQUID magnetometer on powdered samples, in the temperature range 5–400 K; transport measurements were performed by the conventional four-probe technique in a pellet sintered under the synthesis conditions. Magnetotransport measurements were carried out under magnetic fields up to 9 T in a PPMS system from Quantum Design.

3. Results and discussion

$CaVO_3$ was obtained as a black polycrystalline powder. Fig. 1 shows the TG and DTG curves

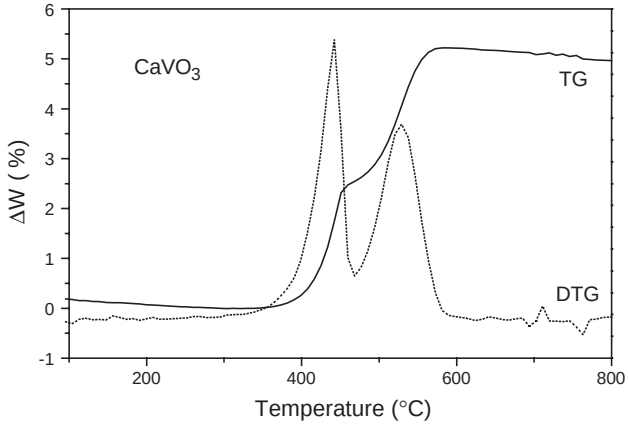

Fig. 1. Thermal analysis (TG and DTG) curves for $CaVO_3$ in an oxidizing air flow.

corresponding to the oxidation process of the sample in an air flow. The weight gain starts above 375°C and ends at around 600°C. The oxidation seems to be formed by two overlapping processes, with DTG temperature peaks at 442°C and 529°C. The total weight gain, of 5.25%, accounts for the incorporation of 0.48(1) oxygen atoms per formula unit, corresponding to the total oxidation of V^{4+} to V^{5+}. The final product above 850°C was identified by X-ray as $Ca_2V_2O_7$, as described by Ueda et al. [10], which does not show a perovskite-like structure. Therefore, the composition of the initial material is $CaVO_{3.02(1)}$, which can be considered as an oxygen-stoichiometric perovskite. The intermediate phase, stable before the second oxidation process, displays an oxygen stoichiometry of about 2.75 oxygens per formula unit; the XRD patterns at this point also correspond to a perovskite structure. Ueda et al. [10] reported on the presence of a metal–insulator transition for this intermediate composition.

3.1. X-ray and neutron powder diffraction

The XRD pattern of $CaVO_3$ compound is characteristic of a perovskite showing well-defined superstructure reflections corresponding to an orthorhombic superstructure, as displayed in Fig. 2. No impurity phases were detected from either XRD or NPD data. The crystal-structure refinement was performed from high-resolution NPD data collected at D2B at room temperature (RT) and with a wavelength $\lambda = 1.594$ Å. The structure was defined in the orthorhombic space group *Pbnm* (No. 62), $Z = 4$, with unit-cell parameters related to $\mathbf{a}_0$ (ideal cubic perovskite, $\mathbf{a}_0 \approx 3.8$ Å) as $\mathbf{a} \approx \mathbf{b} \approx \sqrt{2}\mathbf{a}_0$, $\mathbf{c} \approx 2\mathbf{a}_0$. Ca atoms were located at 4*c* positions, V at 4*b* and oxygen atoms at 4*c* and 8*d* positions, respectively. The oxygen stoichiometry at O1 and O2 positions was checked by refining their occupancy factors; no oxygen vacancies were detected within the standard deviations. An excellent fit between

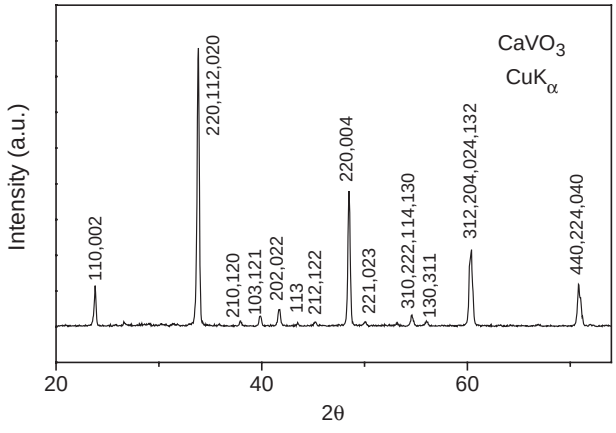

Fig. 2. XRD pattern for $CaVO_3$.

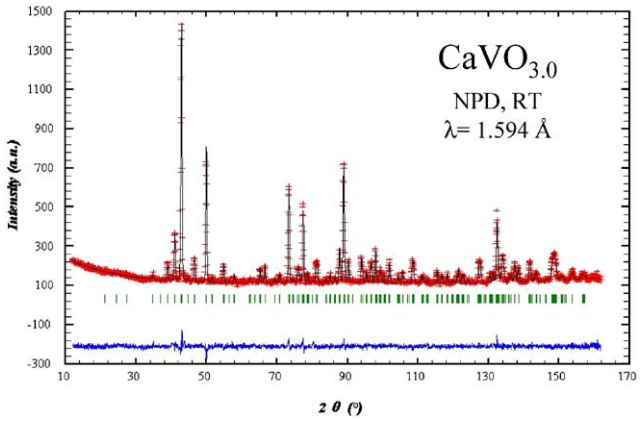

Fig. 3. Observed (crosses), calculated (full line) and difference (bottom) NPD Rietveld profiles for orthorhombic $CaVO_3$ at RT. The series of tick marks corresponds to the allowed Bragg reflections.

the observed and the calculated profiles was obtained, as shown in Fig. 3. Table 1 lists the refined structural and thermal parameters, together with unit-cell parameters refined from NPD data at RT.

Table 2 includes the mean interatomic distances and some selected bond angles. The reasonable fit ($R_{Bragg} \approx 5\%$) obtained for this model allowed us to confirm that the tilting scheme of the VO_6 octahedra corresponds to a $GdFeO_3$-like distortion of the perovskite. The structure of the orthorhombically distorted $CaVO_3$ perovskite contains two unequivalent oxygen positions, which cannot be very accurately determined by XRD diffraction as a strong pseudo-symmetry is present in the patterns. Probably for this reason, the oxygen-stoichiometric material had previously been described as cubic [9], with a unit-cell parameter of 3.79 Å. An NPD study was essential to investigate the subtle structural features of this perovskite, neutrons being more sensitive to the oxygen positions. A view of the crystal structure of $CaVO_3$ is shown in Fig. 4. It is fairly distorted due to the small size of Ca^{2+} cations, which force the VO_6 octahedra to tilt in order to optimize the Ca–O bond distances. The average tilting angle can be estimated as $\phi = (180 - \theta)/2$, where $\theta = \langle V{-}O{-}V \rangle = 159.88°$, then $\phi = 10.05°$.

As shown in Table 2, Ca–O distances in the rather distorted CaO_{12} polyhedron range from 2.37 to 3.098 Å; the effective coordination of Ca^{2+} cations can be considered as eightfold, only considering the bond-lengths below 2.63 Å, with an average $\langle Ca{-}O \rangle_{8\ short}$ value of 2.516 Å which compares well with that expected from the ionic radii sums [12] of 2.52 Å for $^{VIII}Ca^{2+}$ (i.r.: 1.12 Å). For the vanadium-to-oxygen bonds the average distance of 1.915 Å is somewhat shorter than expected, of 1.98 Å for $^{VI}V^{4+}$ ions (i.r.: 0.58 Å). Moreover, the calculation of the valence of the cations present in the solid is enlightening: the phenomenological Brown's

Table 1
Structural parameters for $CaVO_3$ refined in the orthorhombic *Pbnm* space group at room temperature from NPD data

Atom	Site	x	y	z	f_{occ}	B (Å^2)
Ca	4*c*	0.9974(8)	0.0280(6)	1/4	1.0	0.64(7)
V	4*b*	1/2	0	0	1.0	0.3
O1	4*c*	0.0575(5)	0.4907(5)	1/4	0.97(3)	0.43(7)
O2	8*d*	0.7151(4)	0.2856(3)	0.0294(2)	0.98(2)	0.58(5)

Lattice parameters: $a = 5.3219(1)$ Å, $b = 5.3427(1)$ Å, $c = 7.5472(1)$ Å and $V = 214.59$ Å^3.
Discrepancy factors: $R_p = 4.01\%$, $R_{wp} = 5.08\%$ and $R_{Bragg} = 5.30\%$.

Table 2
Main interatomic distances (Å) and angles (deg) for $CaVO_3$

CaO_{12} polyhedron	
Ca–O1	2.888(4)
Ca–O1	2.492(4)
Ca–O1	2.960(5)
Ca–O1	2.376(5)
Ca–O2 (×2)	2.631(3)
Ca–O2 (×2)	2.393(3)
Ca–O2 (×2)	2.604(2)
Ca–O2 (×2)	3.098(3)
⟨Ca–O⟩$_{8\ short}$	2.516(3)
VO_6 octahedron	
V–O1 (×2)	1.9121(5)
V–O2 (×2)	1.920(2)
V–O2 (×2)	1.913(2)
⟨V–O⟩	1.915(2)
V–O1–V	161.33(2)
V–O2–V (×2)	159.16(8)

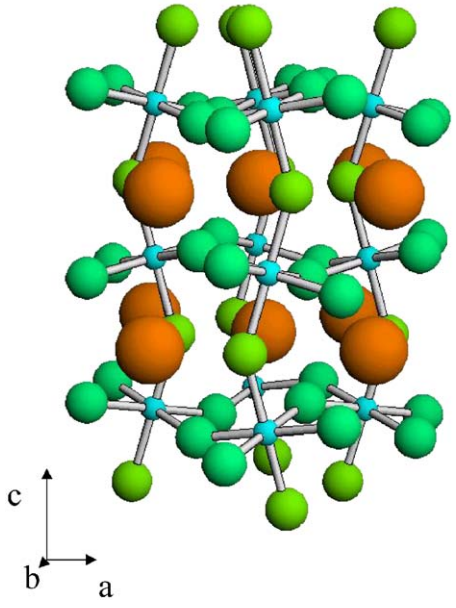

Fig. 4. Schematic representation of the crystal structure of $CaVO_3$ showing the tilting of the VO_6 octahedra. Large spheres represent the Ca atoms.

Bond-Valence Model [13] relates the bond-length r_i and the valence s_i of a bond (for each central atom $v = \Sigma s_i$, $s_i = \exp[(r_0 - r_i)/B]$; $B = 0.37$; $r_0 = 1.967$ and 1.784 for the Ca–O and V–O pairs) [14]. Using this approach the calculated valences in the ionic limit, from the RT data, are 1.99(1) and 4.10(1) for Ca and V cations, respectively. These values suggest that, from the structural parameters, Ca and V cations seem to be close to the divalent and tetravalent oxidation states, as expected.

3.2. Magnetic and transport properties

The susceptibility and reciprocal susceptibility vs. temperature data are shown in Fig. 5a. Above 100 K, the almost temperature-independent observed susceptibility corresponds to the reported Pauli paramagnetic behavior; below this temperature, the susceptibility shows a marked temperature dependence. The total susceptibility $\chi(T)$ can be represented by

$$\chi(T) = \chi_{TIP} + \chi_{dia} + \chi_C(T)$$

with $\chi_C(T) = C/(T - \theta_{Weiss})$, where χ_{TIP}, χ_{dia} and $\chi_C(T)$ are the temperature-independent, diamagnetic and Curie–Weiss terms of the susceptibility. The susceptibility χ_{dia}, to which the ion cores contribute, is estimated to be -51×10^{-6} emu mol^{-1} for $CaVO_3$. The fit to this equation gives a molar Pauli susceptibility of 2.8×10^{-4} emu mol^{-1}, $C = 2.4 \times 10^{-3}$ emu mol^{-1} K and $\theta_{Weiss} = -3.8$ K. For the value of C, the effective number of Bohr magnetons per V atom, p, equals $0.14\,\mu_B/V^{4+}$, which is strongly reduced with respect to the expected free-ion spin-only value of $1.73\,\mu_B/V^{4+}$, according to the high level of electron delocalization expected for this sample. On the other hand, the calculated value for χ_{TIP} is close to that reported for stoichiometric $CaVO_3$ in single crystal samples, of 2.7×10^{-4} emu mol^{-1} [9]. In fact, this value is about five times larger than the expected free-electron Pauli susceptibility. This enhanced value suggests a relatively strong correlation among 3*d* electrons in narrow π^* conduction bands of T_{2g} parentage. A similar behavior has been observed in a number of transition metal oxides which are considered as

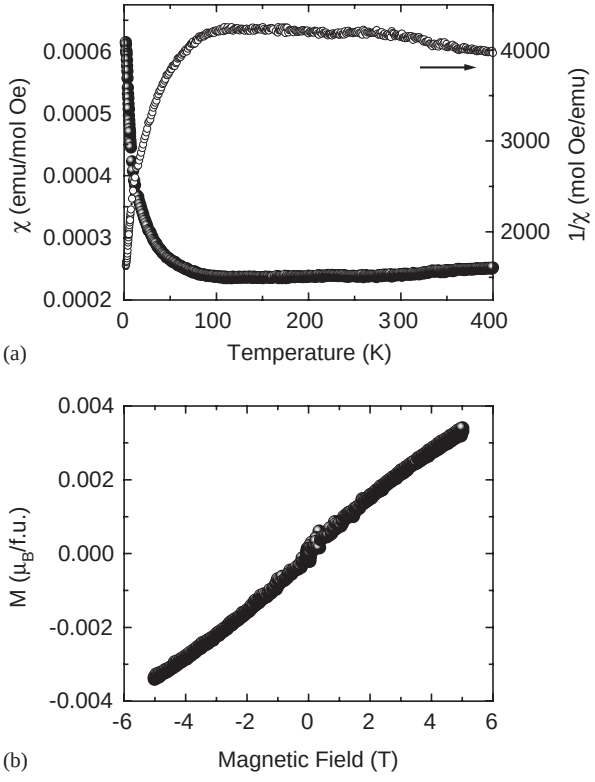

Fig. 5. (a) Temperature dependence of the magnetic susceptibilities and reciprocal susceptibility of $CaVO_3$; and (b) magnetization isotherm at 5 K.

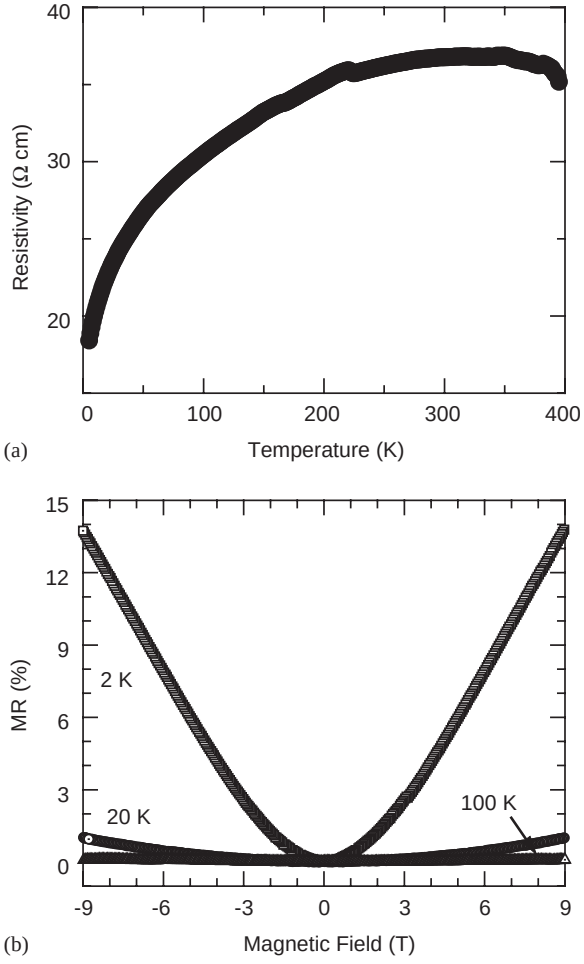

Fig. 6. (a) Thermal variation of the electrical resistivity, and (b) magnetoresistance vs. magnetic field at 2 K.

correlated metallic systems. Typically, $LaNiO_3$ exhibits [15] a Pauli-like paramagnetic susceptibility ($\chi_{TIP} = 5.1 \times 10^{-4}$ emu mol^{-1}) with an additional small Curie-law contribution ($P = 0.17\,\mu_B/Ni^{3+}$); a further example is the perovskite-related oxide $Sr_4V_3O_{9.6}$ [16], with $\chi_{TIP} = 1 \times 10^{-4}$ emu mol^{-1} and $P = 0.22\,\mu_B/V^{4+}$. These figures compare with the values observed for $CaVO_3$. The magnetization isotherm at 5 K (Fig. 5b) shows a linear behavior with the magnetic field, reaching negligible magnetization values of $0.003\,\mu_B$/f.u. at the maximum field of 5 T, thus excluding the presence of weak-ferromagnetic interactions in this system.

The temperature dependence of the electrical resistivity is shown in Fig. 6a. A metallic behavior characterized by a positive slope is observed below 300 K; a relatively high resistivity of $\approx 35\,\Omega$ cm is observed at RT. A $\rho = \rho_0 + AT^2$ law is observed for temperatures below 13 K, as corresponding to a Fermi liquid model, with $\rho_0 = 18.2\,\Omega$ cm and $A = 0.0197\,\Omega$ cm K^{-2}. Regarding the changes in $\rho(T)$ under an external magnetic field, we define $MR(H) = 100 \times [R(H) - R(0)]/R(0)$. Fig. 6b shows the evolution of MR vs. the magnetic field in the $H = 0-9$ T range at 2, 20 and 100 K. A positive magnetoresistance is observed at 2 K, reaching a maximum value of 14% at 9 T. At $T = 2$ K, MR is approximately proportional to the square of the magnetic field; a good fit is obtained for $MR(H) \alpha H^{1.74}$. At $T = 20$ K, the magnetoresistance is reduced at 1% for 9 T, and it is almost negligible for $T = 100$ K. At low temperatures, a much smaller positive magnetoresistance had been previously described for annealed stoichiometric $CaVO_3$ in single crystal form, of 1.2% at $H = 12$ T and 5 K.

In fact, the discovery and design of new material exhibiting large magnetoresistance for applications in magnetoelectronic state is a hot topic in the condensed matter physics and solid-state chemistry. These materials range from artificially engineered magnetic multilayers [17] and granular alloys [18,19] exhibiting negative "giant" magnetoresistance, to the manganese perovskites [2,20] showing negative "colossal" MR. Recently, anomalous positive MR effects were discovered in non-magnetic silver calcogenides [21], metal-doped TiO_2 [22] and perovskite-type manganites [23].

The positive magnetoresistance cannot obviously be understood by the spin-dependent scattering theory, which accounts for the decrease in resistance upon the application of an external magnetic field in a ferromagnetic material. The present kind of positive MR can be attributed to two different origins: (i) that found in normal metals is due to the curving of the carrier trajectory by a magnetic field leading to the observed increase in resistivity, and (ii) quantum interference effects, that take place in systems where the same electrons are responsible for both magnetic properties and electrical conduction. The positive MR observed for $CaVO_3$ perovskite at low-temperatures has probably the same origin to that observed in $La_{0.7}Pb_{0.3}MnO_3$ perovskite manganite between 4.2 and 50 K; this manganite additionally presents the more conventional and well-understood negative MR at higher temperatures [23]. In this case the large positive MR has been interpreted in terms of quantum interference effects originating from the disordered-enhanced Coulomb interactions.

4. Conclusions

We have shown that $CaVO_3$ can be prepared as an homogeneous polycrystalline phase from citrate precursors, decomposed and reduced under an H_2/N_2 flow at a controlled temperature of 900°C. A high-resolution NPD study has been essential to demonstrate that stochiometric $CaVO_{3.0}$ crystallizes with an orthorhombically distorted perovskite structure, containing Ca^{2+} and V^{4+} cations. Above 100 K, this phase shows an enhanced Pauli paramagnetism, with a molar χ_{TIP} of 2.8×10^{-4} emu mol^{-1}, suggesting a strongly correlated electronic system. At lower temperatures, a paramagnetic component with $P = 0.14\,\mu_B/V^{4+}$ is derived from a Curie–Weiss fit, also suggesting the presence of rather weak antiferromagnetic interactions. A positive magnetoresistance, approximately proportional to the square of the magnetic field, is observed at low temperatures, reaching a maximum value of 14% at 9 T and $T = 2$ K. This value is substantially larger than that previously described for annealed stoichiometric $CaVO_3$ in single crystal form, and can be interpreted as a result of quantum interference effects.

Acknowledgments

H. Falcón is grateful to the Spanish Secretaría de Estado de Educación y Universidades for a grant he received. Financial support from CICYT, Spain, under Project MAT2001-0539 is also acknowledged. The authors are grateful to ILL for making all facilities available.

References

[1] J.G. Bednorz, K.A. Muller, Z. Phys. B 64 (1986) 189.
[2] Y. Tokura (Ed.), Colossal Magnetoresistive Oxides, Gordon and Breach, London, 2000.
[3] N.F. Mott, Metal–Insulator transitions, Taylor and Francis, London, 1990.
[4] F. Iga, Y. Nishihara, J. Phys. Soc. Japan 61 (1992) 1867.
[5] J. García-Jaca, J.I.R. Larramendi, M. Insausti, M.I. Arriourtua, T. Rojo, J. Mater. Chem. 5 (1995) 1995.
[6] B.L. Chamberland, P.S. Danielson, J. Solid State Chem. 3 (1971) 243.
[7] J.B. Goodenough, Transition metal oxides, Prog. Solid State Chem. 5 (1971) 149.
[8] I.H. Inoue, K. Morikawa, H. Fukuchi, T. Tsujii, F. Iga, Y. Nishihara, Physica B 194 (1994) 1067 (Amsterdan).
[9] A. Fukushima, F. Iga, I.H. inoue, K. Murata, Y. Nishihara, J. Phys. Soc. Japan 63 (1994) 409.
[10] Y. Ueda, J. Solid State Chem. 135 (1998) 36.
[11] J. Rodríguez-Carvajal, Physica B 192 (1993) 55 (Amsterdam).
[12] R.D. Shannon, Acta Crystallogr. A 32 (1976) 751.
[13] I.D. Brown, in: M. O'Keefe, A. Navrotsky (Eds.), Structure and Bonding in Crystals, Vol. 2, Academic Press, New York, 1981, pp. 1–30.
[14] N.E. Brese, M. O'Keefe, Acta Crystallogr. B 47 (1991) 192.
[15] K. Sreedhar, J.M. Honig, M. Darwin, M.M. McElfresh, P.M. Shand, J. Xu, B.C. Crooker, J. Spalek, Phys. Rev. B 46 (1992) 6382.
[16] N. Suzuki, T. Noritake, N. Yamamoto, T. Hioki, Mater. Res. Bull. 26 (1991) 75.
[17] M.N. Baibich, J.M. Broto, A. Fert, F. Nguyen Van Dau, F. Petroff, Phys. Rev. Lett. 61 (1988) 2472.
[18] A.E. Berkowitz, J.R. Mitchell, M.J. Carey, A.P. Young, S. Zhang, F.E. Spada, F.T. Parker, A. Hutten, G. Thomas, Phys. Rev. Lett. 68 (1992) 3745.
[19] J.Q. Xiao, J. Samuel Jiang, C.L. Chien, Phys. Rev. Lett. 68 (1992) 3749.
[20] S. Jin, T.H. Tiefel, M. McCormack, R. Fastnacht, R. Ramesh, L.H. Chen, Science 264 (1994) 413.
[21] R. Xu, A. Hussmann, T.F. Rosenbaum, M.L. Saboungi, J.E. Enderby, P.B. Littlewood, Nature 390 (1997) 57 (London).
[22] Y. Matsumoto, M. Murakami, T. Shono, T. Hasegawa, T. Fukumura, M. Kawasaki, P. Ahmet, T. Chikyow, S. Koshihara, H. Koinuma, Science 291 (2001) 854.
[23] P. Chen, D.Y. Xing, Y.W. Du, Phys. Rev. B 64 (2001) 104402.